Vol 17 No 9, September 2008
1674-1056/2008/17(09)/3464-07

Chinese Physics B

© 2008 Chin. Phys. Soc.
and IOP Publishing Ltd

The high deposition of microcrystalline silicon thin film by very high frequency plasma enhanced chemical vapour deposition and the fabrication of solar cells*

Chen Yong-Sheng(陈永生)[a)b)†], Wang Jian-Hua(汪建华)[c)], Lu Jing-Xiao(卢景霄)[b)], Zheng Wen(郑 文)[b)], Gu Jin-Hua(谷锦华)[b)], Yang Shi-E(杨仕娥)[b)], Gao Xiao-Yong(郜小勇)[b)], Guo Xue-Jun(郭学军)[b)], Zhao Shang-Li(赵尚丽)[b)], and Gao Zhe(高 哲)[b)]

[a)] *Institute of Plasma Physics, Chinese Academy of Sciences, Hefei* 230031, *China*
[b)] *Key Laboratory of Material Physics, Department of Physics, Zhengzhou University, Zhengzhou* 450052, *China*
[c)] *Department of Materials Science and Engineering, Wuhan Institute of Technology, Wuhan* 430073, *China*

(Received 24 December 2007; revised manuscript received 7 January 2008)

This paper reports that the intrinsic microcrystalline silicon (μc-Si:H) films are prepared with plasma enhanced chemical vapour deposition from silane/hydrogen mixtures at 200°C with the aim to increase the deposition rate. An increase of the deposition rate to 0.88 nm/s is obtained by using a plasma excitation frequency of 75 MHz. This increase is obtained by the combination of a higher deposition pressure, an increased silane concentration, and higher discharge powers. In addition, the transient behaviour, which can decrease the film crystallinity, could be prevented by filling the background gas with H_2 prior to plasma ignition, and selecting proper discharging time after silane flow injection. Material prepared under these conditions at a deposition rate of 0.78 nm/s maintains higher crystallinity and fine electronic properties. By H-plasma treatment before i-layer deposition, single junction μc-Si:H solar cells with 5.5% efficiency are fabricated.

Keywords: chemical vapour deposition, plasma deposition, solar cells, crystallinity
PACC: 7280N, 7830G, 8115H

1. Introduction

Microcrystalline silicon (μc-Si:H) is used in thin film single junction μc-Si:H and amorphous silicon (a-Si:H)/μc-Si:H tandem solar cells because of its lower band gap, and hence the optical absorption in the near infrared region is higher.[1−4] However, we estimate that for a sufficient absorption, a film thickness of several microns is necessary, which is a critical point, because in general the deposition rates of μc-Si:H in standard plasma enhanced chemical vapour deposition (PECVD) are very low. Increasing growth rate of μc-Si:H requires reasonably high discharge power for high dissociation of the reactant gases, leading to higher sheath voltages, and thus higher ion energy. High-energy ions impinging on the growth surface, however, are considered to be detrimental to the quality of μc-Si:H, causing defect formation and deterioration in crystallinity.[5,6] Therefore, suppressing the high-energy ions in the plasma is of particular necessity at a high deposition rate (R_D). Effective methods to reduce ion energies while maintaining high deposition rates are (i) very high frequency (VHF) excitation of the discharge, where lower peak-to-peak voltages for a given discharge power result in lower maximum-ion energies,[7−9] and (ii) high working pressure (p_{depo}) with an increased discharge power, where ion energies are reduced by multiple collisions in the plasma sheath.[10,11] Recently, also combinations of VHF-PECVD and high working pressure have been investigated.[12−14] In addition, transient depletion of source gases can play an important role in materials processing, particularly during the initial phase of thin film synthesis in which nucleation takes place and the interface is formed. Donker *et al*[15] demonstrated that high H_2 flow generally applied during deposition of μc-Si:H in the 13.56 MHz high pressure depletion (HPD) regime is needed to suppress SiH_4 back diffusion (an initial diffusion flux of SiH_4 from the reactor's dead volume back into the plasma),

*Program supported by the State Key Development Program for Basic Research of China (Grant No 2006CB202601), and Basic Research Project of Henan Province in China (Grant No 072300410140).
†Corresponding author. E-mail: chysh2003@zzu.edu.cn

which caused the decrease of Raman crystallinity in film. Therefore, there is interest in investigating the effect of SiH_4 back diffusion to the film crystallinity and microstructure under HPD-VHF plasma.

In this paper we present a study of the different gas conditions prior to plasma ignition on the growth and microstructure of μc-Si:H films, and report on further studies of such a combination of VHF-PECVD at 75 MHz at high working pressures for the growth of μc-Si:H at higher deposition rates and fabricate single junction μc-Si:H solar cells at higher intrinsic film deposition rate. In p-i-n solar cells, the i/p interface properties can affect the cell performance and the stability. To provide a good grain boundary passivation and a compact material structure in i/p interface, different times of H-plasma treatment after p-layer deposition are used.

2. Experimental details

The p, i, and n layers of the μc-Si:H solar cells were deposited in individual chambers of a cluster-tool deposition system[16] by PECVD to form p-i-n single-junction diodes. Figure 1 shows a schematic picture of the deposition chamber. The electrode configuration consists of a 31.0 cm diameter powered electrode. Substrate size is 5 cm × 5 cm. The electrode distance is 15 mm. A metal shield around the electrodes to prevent deposition on the chamber walls, as indicated in Fig.1, can be removed for discharge adjustment. The gas supply is realized through a showerhead arrangement.

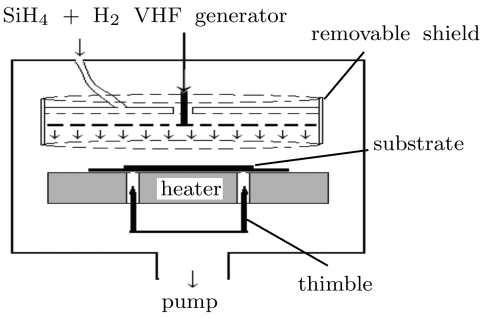


Fig.1. Schematic picture of the PECVD deposition chamber.

Solar cells are deposited on ZnO/SnO_2 bi-layer-coated glass substrates.[17] Substrate temperatures are 150, 200, 170°C for p-, i-, and n-layer depositions. The μc-Si:H i layers were deposited with VHF-PECVD at 75 MHz. The μc-Si:H p and a-Si:H n layers were deposited with conventional RF (radio frequency)-PECVD at 13.56 MHz.[18] The H-plasma treatment was applied to p-layers in the VHF chamber. In order to illustrate the impact of the hydrogen plasma, a series of different exposure times of the p-layer, as exposed to hydrogen bombardment by the hydrogen plasma, was carried out. The applied hydrogen plasma conditions were chosen in view of yielding a low energy ion-bombardment[19] ($p_{\mathrm{depo}} = 133$ Pa, $Fl_{(\mathrm{H2})} = 200$ sccm, $P_{\mathrm{VHF}} = 40$ W at $f = 75$ MHz) needed to avoid the etching of the p-layer, i.e. by sputtering. The silane concentration (SC), SC = $[SiH_4]$ / ($[SiH_4]$+$[H_2]$), defined by the gas-flow ratio of silane and hydrogen, plasma power and deposition pressure were varied in order to obtain higher deposition rate.

The detailed deposition parameters of the intrinsic films are shown in Table 1, in which Fl_{total} means the total gas flow ($[SiH_4] + [H_2]$).

The deposition time for i-layers was adjusted to obtain a thickness of approximately 0.8 μm. The thickness of the solar cells was measured with a step profiler. The deposition rate was calculated from the thickness measurement in the centre of the substrate. The area of individual solar cells is defined by the 5 mm × 5 mm evaporated Al back contact and consists of a 30 nm thick microcrystalline p-layer, a 1.5 μm-thick microcrystalline i-layer, and a 50 nm thick amorphous n-layer. The J–V characteristics of the solar cells, i.e., efficiency, open-circuit voltage V_{OC}, fill factor FF, and short-circuit current density J_{SC}, were measured under AM1.5 illumination at 25°C.

To study the effect of transient depletion on the film microstructure, several series of samples were deposited at different gas backgrounds prior to plasma ignition in two gas mixture SC ($SiH_4/(SiH_4 + H_2)$ = 2%, 4%), each series at a fixed VHF power in 100 W. The different gas conditions in the H_2 backgrounds were achieved by adjusting the time intervals between SiH_4 flow injecting into the chamber and plasma ignition. The deposition time is started from the moment of plasma ignition and maintains deposition for 1–2min, and the spectroscopic ellipsometry (SE) is used to provide information on crystallinity vs film thickness. SE spectra were analysed using the Bruggeman effective medium approximation (BEMA) assuming the μc-Si:H films consisting of microcrystalline and amorphous silicon phases and voids. The model describing the films consists of (1) the interface with the substrate; (2) the bulk microcrystalline film; (3) the 'growth-front' and rough surface layer.

The dark conductivity (σ_D) and photoconductivity (σ_{ph}) were measured at room temperature using coplanar Al contacts by 1 mm interval using Keithley 6517 multimeter with or without AM1.5 illumination. The coplanar temperature-dependent dark conductivity $\sigma_D(T)$ measured on the samples over a wide temperature range (300–450 K) in a vacuum chamber shows an activated behaviour: $\sigma_D = \sigma_0 e^{-E_a/kT}$, where σ_0 is known as the conductivity prefactor and E_a as activation energy. To study the crystallinity of the films, Raman spectra were measured in a backscattering configuration using a Raman spectrometer with a He–Ne laser exciting source. 5.0 mW output power and 632.8 nm wavelengths were used in the measurements. The crystalline ratio X_c was obtained as[20]:

$$X_c = (I_{520} + I_{510})/(I_{520} + I_{510} + I_{480}),$$

where I_{520} and I_{510} are the intensities of crystalline like peaks whereas I_{480} is that of amorphous like peak of the transverse optic Si–Si vibrations in the Raman spectra. Scan electron microscopy (SEM) is used to investigate the section morphology of boron-doped microcrystalline layers.

Table 1. Deposition parameters of the intrinsic films.

series name	SC/%	Fl_{total}/sccm	P_{VHF}/W	p_{depo}/Pa	T_{sub}/°C
Insc1	2–5	250	140	300	200
Insc2	2–4	300	140	350	200
InPp	4	250	60–140	133–350	200
Cellsc	4	250	140	300	200

3. Results

3.1. The transient depletion effect

Figure 2 shows the Raman crystallinity of μc-Si:H films deposited under different gas condition in the H_2 backgrounds. The abscissa in the figure represents the time intervals between silane injection and plasma ignition: '0' means the plasma is ignited at the moment of silane inpouring into the chamber; other points indicate that plasma is ignited after silane has injected into the chamber for corresponding time. The Raman crystallinity of μc-Si:H films increases first, then decreases with the time prolonging between silane injection and plasma ignition. The highest crystallinity is obtained at time interval between silane injection and plasma ignition of 20 s for SC = 2%, and of 30 s for SC = 4%. Under same time interval, crystallinity decreases with the increase of silane concentration. Figure 3 shows the deposition rate in the initial film growth stage under different gas conditions. The trends of deposition rate are reversed with that of film crystallinity, and increase with the delay of plasma ignition.

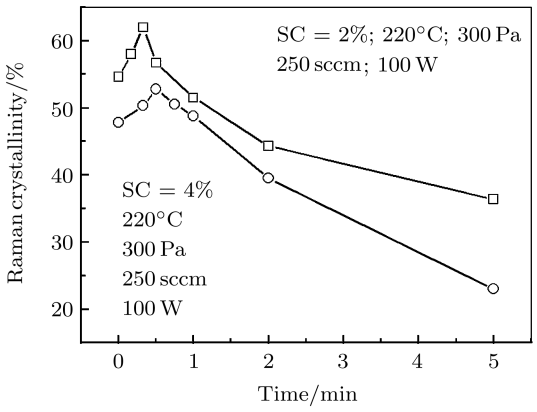


Fig.2. The Raman crystallinity of films deposited under different gas conditions.

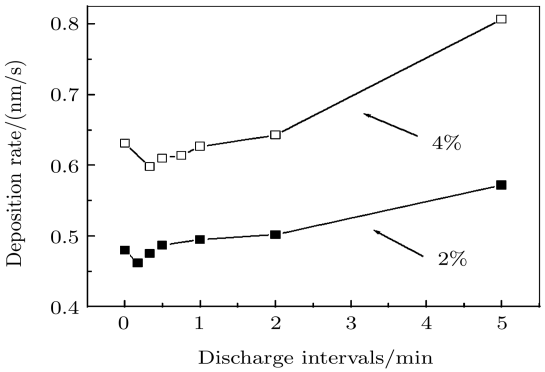


Fig.3. The variation of deposition rate in the initial plasma ignition stage under different gas conditions.

The SiH_4 back diffusion is responsible for the experimental results. The effect of SiH_4 back diffusion on the dust formation process in the plasma[21] and the preventing method[15] had been discussed. This back diffusion, as one transient behaviour, can be explained in terms of a transformation of the gas composition, as sketched in Fig.4. In the standard deposition process,

the entire reactor is filled with the SiH_4/H_2 gas mixture before plasma ignition (Fig.4(a)), whereas in the stable situation after plasma ignition (Fig.4(d)) the SiH_4 is heavily depleted [22−25] and the reactor is predominantly filled with H_2. During the transformation, the SiH_4 depletion in the plasma zone (Fig.4(b)) drives a diffusion flux of SiH_4 from the reactor's dead volume back into the plasma[26] (Fig.4(c)). The back diffusion of SiH_4 increases the real density of silane in plasma, leading to the decrease of film crystallinity, and the increase of amorphous incubation layer's thickness and of the deposition rate. The SiH_4 diffusion flux should be proportional to the initial SiH_4 density in the reactor. So, the effect of this back diffusion becomes more serious with the delay of plasma ignition and the increase of silane concentration in the feed gases, as shown by experimental results. By designing a dedicated plasma ignition procedure involving a H_2 purging step prior to ignition, the influence of the transient depletion induced incubation layer can be succeeded in elimination, and is applied in the followed deposition process.

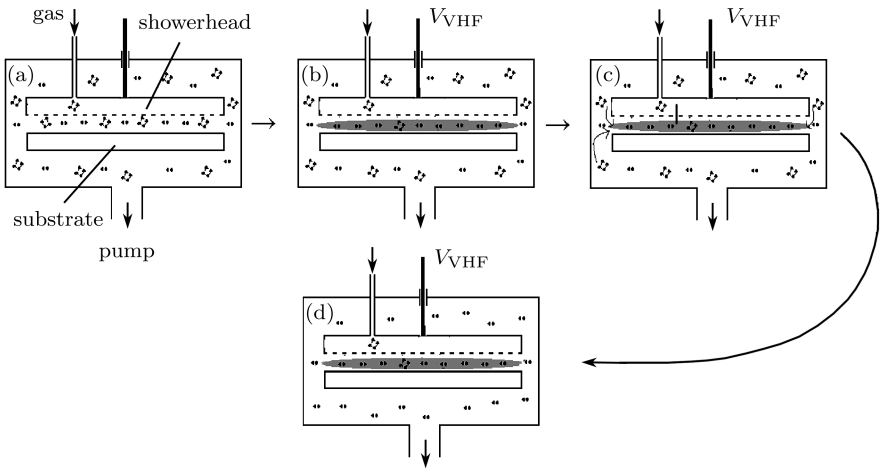
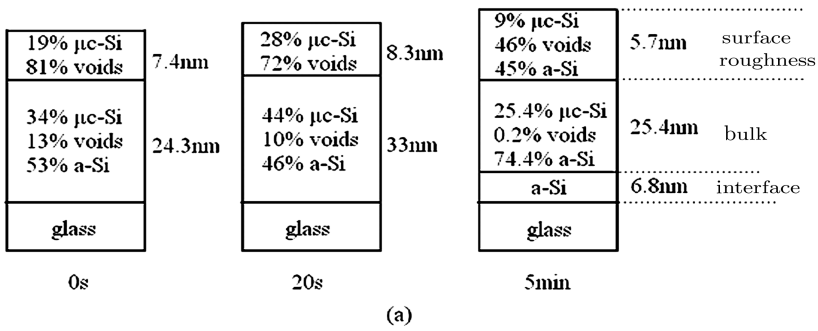


Fig.4. Schematic representation of the sequence of processes that occur after plasma ignition in the standard process: (a) stable situation before plasma ignition; (b) plasma ignition and initial SiH_4 depletion in the plasma zone; (c) SiH_4 back diffusion and purging; (d) stable situation after plasma ignition.

The best-fit corresponding BEMA models showing the microstructure of films are reported in Fig.5. The microcrystallinity of the samples can be inferred by the presence in the SE spectra of the E_1 and E_2 critical points. It is interesting noting that under constant silane concentration: 1) The crystalline volume fractions in bulk and surface layers increases first with the delay of plasma ignition behind the silane flow injection and gets a maximum at 20 s or 30 s, then decreases with further increasing of delay time. 2) The voids volume fractions are much lower in bulk layers than in surface layer, and decrease with the decreasing of crystallinity in corresponding layers. However, the voids volume fractions are high in the bulk layers at 0 s time interval. 3) The thick interface a-Si layers appear at longer time intervals. In addition, the crystallinity decreases with the increasing of silane concentration. The ellipsometric analysis indicates that changing gas condition before plasma ignition is effective in suppressing removal of the amorphous interface layer at the onset of crystallite nucleation.



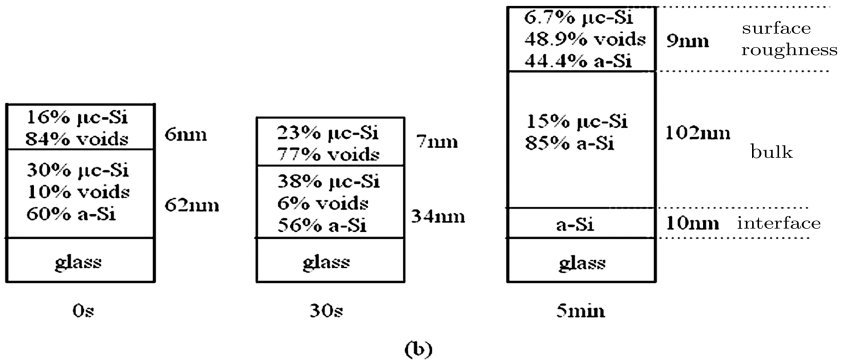


Fig.5. The best-fit BEMA models of the imaginary part, $\langle\varepsilon_2\rangle$, of the pseudodielectric function of μc-Si:H films deposited under different time intervals at (a) SC = 2%; (b) SC = 4%.

3.2. The high deposition rate of intrinsic μc-Si:H films

Figure 6 shows the deposition rates and Raman crystallinity for i-layers deposited at an excitation frequency of 75 MHz as a function of the SC with various total gas flow ($Fl_{\rm total}$) and deposition pressure. As expected, the deposition rate increases with the SC and $Fl_{\rm total}$, $p_{\rm depo}$. At SC = 2% and with lower $Fl_{\rm total}$ and $p_{\rm depo}$, we have a low deposition rate of about 0.4 nm/s and material with a crystalline volume fraction of 76%. Increasing the SC to 5% leads to an increase of the deposition rate to 0.88 nm/s, but the film has a larger amorphous phase fraction. Figure 7 shows the variation of dark conductivity with temperature. The $\sigma_{\rm D}$ and $\sigma_{\rm ph}$ for SC = 3% and 4% are 3.11×10^{-6} S/cm, 2.04×10^{-4} S/cm and 2.83×10^{-6} S/cm, 1.01×10^{-4} S/cm, which yield activation energies of $E_{\rm a}=0.385$ eV and $E_{\rm a}=0.442$ eV, respectively. Increasing $Fl_{\rm total}$ and $p_{\rm depo}$ in Fig.6 results in an increase of the rate, but the decrease of Raman crystallinity.

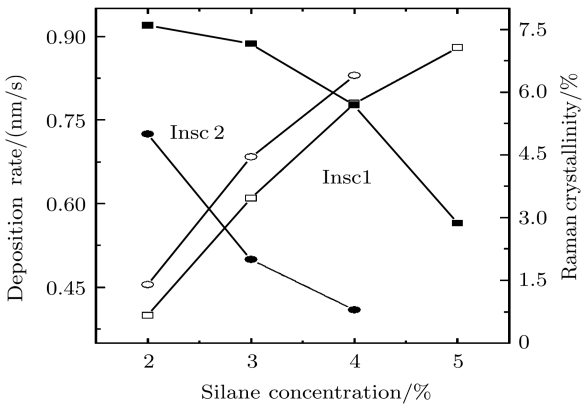


Fig.6. Deposition rate and Raman crystallinity as a function of the silane concentration for films deposited at various $Fl_{\rm total}$ and $p_{\rm depo}$.

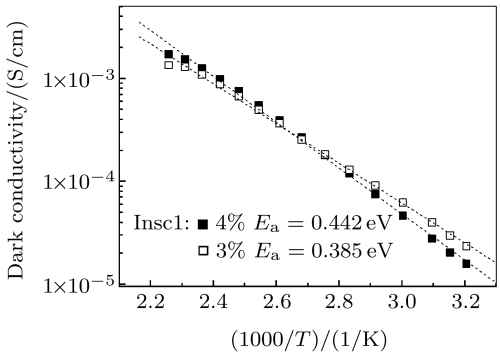


Fig.7. The variation of dark conductivity with temperature at various silane concentrations. Lines are drawn as guides for the eye.

Figure 8 shows a μc-Si:H formation map on VHF power and deposition pressure plane. The areas of close and open triangle represent crystalline volume fraction and deposition rate, respectively, in μc-Si:H deposited under given conditions at SC = 4%. As is

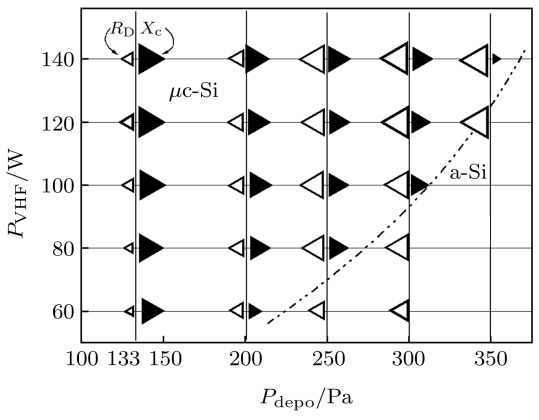


Fig.8. Formation map of μc-Si:H in VHF power and deposition pressure plane. The areas of close and open triangle represent crystalline volume fraction and deposition rate, respectively. The dashed line in the figure means μc-Si:H/a-Si:H transition.

seen in the figure, good crystallinity is obtained under high power and low pressure conditions. At constant p_{depo}, an increase in the P_{VHF} did hardly increase the deposition rate, but did increase the crystallinity of the films. This results in a shift of the μc-Si:H/a-Si:H transition to higher p_{depo}, and therefore leads to a higher R_{D} for the optimum films. On the other hand, an increase in the p_{depo} at constant P_{VHF} did lead to a higher R_{D}, but lower crystallinity. With this shift of the μc-Si:H/a-Si:H transition at higher p_{depo}, the R_{D} for the optimum films decreased.

3.3. The fabrication of solar cells

Lots of researches demonstrate that optimum solar cells are always found to be close to the transition from microcrystalline to amorphous growth, with a crystallinity of about 60%.[13,27] So, Cellsc (R_{D} = 0.78 nm/s, X_{c} = 56.9%) is selected as the optimum conditions to deposit the i-layers of solar cells. Under higher deposition rate, i/p interface properties become very important. In order to improve the i/p interface properties, H-plasma treatment is used before μc-Si:H i-layers deposition. Figure 9 shows the effect of H-plasma treatment to the characteristics of single junction μc-Si:H thin film solar cells. The V_{OC} and J_{SC} of solar cells increased with the increasing H-plasma treating time. After 20 min H-plasma treatment, the efficiency of solar cells increased more than 20%, and highest efficiency of 5.5% was obtained (see Fig.10).

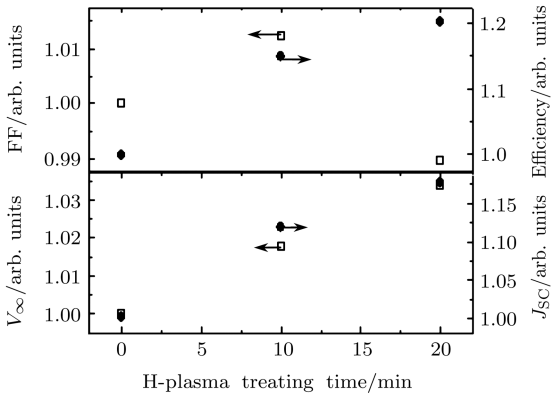


Fig.9. The effect of H-plasma treatment to the characteristics of μc-Si:H thin film solar cells.

It was suggested that H-plasma treatment provides a good grain boundary passivation and a compact material structure in i/p interface,[28] and increases the crystallinity of p-layers.[29] To make it clear may need further research. Figure 11 shows SEM section micrograph of μc-Si:H single junction solar cell. It can be clearly seen that the growth of μc-Si:H film presents certain column characteristic.

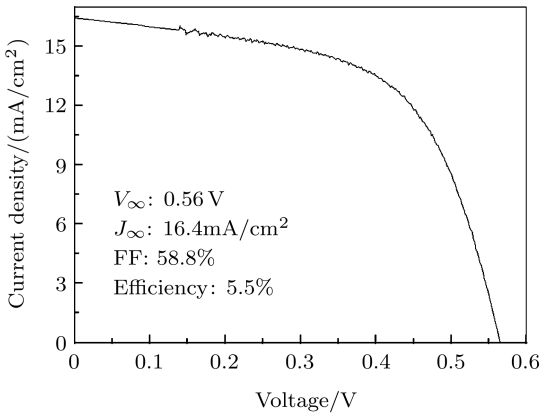


Fig.10. The current-voltage characteristic of single junction microcrystalline silicon solar cells.

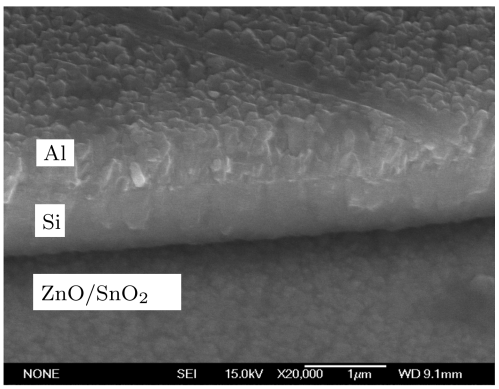


Fig.11. The SEM micrograph of μc-Si:H single junction solar cell.

4. Conclusions

It has been shown that by changing time intervals between the silane injection and plasma ignition in a H_2 background, SiH_4 back diffusion can be suppressed and high-quality μc-Si:H can be deposited, and the deposition rate of μc-Si:H increases combining high plasma excitation frequencies, high plasma power, higher deposition pressure and high SCs. Using these conditions, we can improve the structure with respect to the crystalline volume fraction. The high deposition rate of 0.78 nm/s material maintains good electronic properties with dark conductivities of 2.83×10^{-6} S/cm. Using this film as i-layer of single junction μc-Si:H thin film solar cells, and applying H-plasma treatment before its deposition, we obtain highest efficiency of 5.5%.

References

[1] Kondo M, Nasuno Y, Mase H, Wada T and Matsuda A 2002 *J. Non-Cryst. Solids* **299–302** 108

[2] Vetterl O, Finger F, Carius R, Hapke P, Houben L, Kluth O, Lamberts A, Much A, Bech B and Wanger H 2000 *Sol. Energy Mat. Sol.* C **62** 97

[3] Shah A V, Meier J and Graf U 2003 *Sol. Energy Mat. Sol.* C **78** 469

[4] Gao X Y, Li R, Chen Y S, Lu J X, Liu P, Feng T H, Wang H Y and Yang S 2006 *Acta Phys. Sin.* **55** 98 (in Chinese)

[5] Matsuda A 1983 *J. Non-Cryst. Solids* **59–60** 767

[6] Vepøek S, Sarrot F A, Rambert S and Taglauer E 1989 *J. Vac. Sci. Technol.* A **7** 2614

[7] Gao Y T, Zhang X D, Zhao Y, Sun J, Zhu F, Wei C C and Chen F 2006 *Chin. Phys.* **15** 1110

[8] Yang H D and Su Z Y 2006 *Chin. Phys.* **15** 1374

[9] Wu Z M, Lei Q S, Geng X H, Zhao Y, Sun J and Xi J P 2006 *Chin. Phys.* **15** 1320

[10] Guo L, Kondo M, Fukawa M, Saitoh K and Matsuda A 1998 *Jpn. J. Appl. Phys.* Part 2 **37** L1116

[11] Roschek T, Repmann T, Müller J, Rech B and Wagner H 2002 *J. Vac. Sci. Technol.* A **20** 492

[12] Gordijn A, Hodakova L, Rath J K and Schropp R E I 2006 *J. Non-Cryst. Solids* **352** 1868

[13] Mai Y, Klein S, Carius R, Wolff J, Lambertz A and Finger F 2005 *J. Appl. Phys.* **97** 114913

[14] van den Donker M N, Kilper T, Grunsky D, Rech B, Houben L, Kessels W M M and van de Sanden M CM 2007 *Thin Solid Films* **515** 7455

[15] van den Donker M N, Rech B, Finger F, Kessels W M M and van de Sanden M CM 2005 *Appl. Phys. Lett.* **87** 263503

[16] Chen Y S, Gao X Y, Yang S, Lu J X and Gu J H 2007 *Acta Phys. Sin.* **56** 4122

[17] Chen Y S, Wang J H, Lu J X, Yang G, Gao X Y and Yang S 2007 *Chin. J. Semicond.* **28** 1005

[18] Chen Y S, Yang S, Wang J H, Lu J X, Gao X Y, Gu J H, Zheng W and Zhao S L 2008 *Chin. Phys.* B **17** 1394

[19] Godet C, Layadi N and Roca I Cabarroocas P 1995 *Appl. Phys. Lett.* **66** 3146

[20] Kalache B 2003 *J. Appl. Phys.* **93** 1262

[21] Findeisen E, Feidenhans E R, Vigild M E, Clausen K N, Hansen J B, Bentzon M D and Goff J P 1994 *J. Appl. Phys.* **76** 4636

[22] Sorokin M, Kroesen G M W and Stoffels W W 2004 *IEEE Trans. Plasma Sci.* **32** 731

[23] Roschek T, Rech B, Müller J, Schmitz R and Wagner H 2004 *Thin Solid Films* **451–452** 466

[24] Guo L, Kondo M, Fukawa M, Saitoh K and Matsuda A 1998 *Jpn. J. Appl. Phys.* Part 2 **37** L1116

[25] Rech B, Roschek T, Repmann T, Müller J, Schmitz R and Appenzeller W 2003 *Thin Solid Films* **427** 157

[26] Amanitides E, Hammad A, Katsia E and Mataras D 2005 *J. Appl. Phys.* **97** 073303

[27] Losurdo M, Giangregorio M, Sacchetti A, Capezzuto P, Bruno G and Giorgis F 2006 *Appl. Surf. Sci.* **253** 287

[28] Zhang X D, Zhao Y, Gao Y T, Zhu F, Wei C C, Sun J, Geng X H and Xiong S Z 2005 *Acta Phys. Sin.* **54** 4874 (in Chinese)

[29] Yamamoto K, Nakajima A, Yoshimi M, Sawada T, Fukuda S, Suezaki T, Ichikawa M, Koi Y, Goto M, Meguro T, Matsuda T, Kondo M, Sasaki T and Tawada Y 2004 *Solar Energy* **77** 939